


Article

Impact of Land Cover and Leaf Area Index on BVOC Emissions over the Korean Peninsula

Youjung Jang ¹, Yangdam Eo ² , Meongdo Jang ³, Jung-Hun Woo ^{1,2,*}, Younha Kim ^{1,4,*}, Jae-Bum Lee ⁵ and Jae-Hyun Lim ⁵

¹ Department of Advanced Technology Fusion, Konkuk University, Seoul 05029, Korea; zaharyu@gmail.com

² Civil and Environmental Engineering, College of Engineering, Konkuk University, Seoul 05029, Korea; eoandrew@konkuk.ac.kr

³ Korea Meteorological Institute, Seoul 03735, Korea; mdjang@kmiti.or.kr

⁴ International Institute for Applied Systems Analysis, 2361 Laxenburg, Austria

⁵ National Institute of Environmental Research, Incheon 22689, Korea; gercljb@korea.kr (J.-B.L.); d14earth@korea.kr (J.-H.L.)

* Correspondence: jwoo@konkuk.ac.kr (J.-H.W.); pinktokkya@naver.com (Y.K.); Tel.: +82-2-453-2706 (J.-H.W.)

Received: 2 June 2020; Accepted: 25 July 2020; Published: 30 July 2020



Abstract: Biogenic volatile organic compound (BVOCs) emissions are the largest VOC emission source globally, and are precursors to ozone and secondary organic aerosols, both of which are strong, short-lived climate pollutants. BVOC emissions are usually estimated using the Model of Emissions of Gases and Aerosols from Nature (MEGAN), which requires Plant Functional Types (PFTs) and Leaf Area Indexes (LAIs) as inputs. Herein, the effects of refined input data on regional BVOC emission estimates are analyzed. For LAIs, lower resolution MODerate-resolution Imaging Spectroradiometer (MODIS), and higher spatio-temporal resolution Spatial and Temporal Adaptive Reflectance Fusion Model (STARFM) LAI were generated. For PFTs, local land cover maps were developed, in addition to MODIS PFT. In South Korea, annual emissions of isoprene and monoterpenes in 2015 were estimated as 384 and 160 Gg/year, respectively, using STARFM LAI and Local PFT (Case 4). For North Korea, 340 Gg/year isoprene and 72 Gg/year monoterpenes emissions were estimated using STARFM LAI and MODIS PFT. These estimates were 14–110% higher than when using MODIS LAI and MODIS PFT (Case 1). Inter-comparison with satellite-based inverse isoprene emission estimates from GlobEmission shows 32% (North Korea) to 34% (South Korea) overestimation in bottom-up data. Our new vegetation inputs improve MEGAN performance and resulting BVOC emission estimations. Performance of Weather Research and Forecasting (WRF) meteorological modeling requires improvement, especially for solar radiation, to avoid overestimation of isoprene emissions.

Keywords: biogenic volatile organic compounds (BVOC); plant functional types; leaf area index; Model of Emissions of Gases and Aerosols from Nature (MEGAN); South Korea; North Korea

1. Introduction

Climate change theory suggests that ecosystems can become potentially large volatile organic compound (VOC) sources [1]. Biogenic VOCs (BVOCs) emitted from plants are involved in ozone generation through photochemical reactions, and are precursors for the formation of secondary organic aerosols [2–4]. VOC emissions from vegetation are comparable to those emitted from anthropogenic sources, with relative emission values varying across regions and seasons [5]. The Korean Peninsula is located in the far east of the Eurasian continent where many industrial countries are located, and anthropogenic emissions are regionally very strong. The combination of these anthropogenic VOCs and natural BVOCs acts as a precursor to ozone and secondary organic aerosol formation.

In Korea, 70% of the total area is composed of vegetation, such as forests. Based on a joint National Aeronautics and Space Administration (NASA) and Korean National Institute of Environmental Research (NIER) KORUS-AQ 2016 aircraft field campaign, NO_x from urban areas moves to regions where BVOCs are generated, promoting ozone formation [6]. In order to quantify the BVOCs that affect air quality, emission data or accurate emission estimates are required.

Emission models are usually used to estimate BVOC emissions. The Model of Emissions of Gases and Aerosols from Nature (MEGAN), developed by the National Center for Atmospheric Research (NCAR) in the United States, is a well-known emission modeling system [7,8]. For input data, MEGAN uses plant functional type (PFT), which refers to vegetation distribution, the leaf area index (LAI), which indicates the amount of BVOC-emitting foliage per unit ground area, and meteorological conditions. However, to estimate emissions accurately, it is necessary to use representative input data [7]; over the period 2000–2012, several studies used MEGAN to estimate global emissions [7–10]. For Asia, a case study of isoprene emission investigated the link with land use change over the period 1979–2012 [11]; emissions from July and August were calculated and compared with satellite data in 2000 [12]. These continental-scale studies have given valuable insights into the broad distribution of BVOCs emissions, but still have limitations for smaller countries, like North and South Korea, owing to low spatial resolutions.

This study was conducted to understand the effect of using different PFT and LAI datasets as vegetation input data in a BVOCs emission model, when trying to quantify realistic BVOC emission estimates for the Korean Peninsula. The effect of meteorological modeling performance as an input to MEGAN v2.1 emissions model was also discussed.

2. Methodology

2.1. Biogenic VOC Emissions Model

The algorithm for estimating biogenic emissions in MEGAN is shown in Equation (1). The main components can be divided into two categories: calculation of emission responses to vegetation condition, and calculation of standard vegetation emission factors,

$$F_i = \gamma_i \sum \varepsilon_{i,j} \chi_j, \quad (1)$$

where F_i is the emissions of chemical species i ($\mu\text{g}/\text{m}^2 \text{ h}$), γ_i is the emissions activity of chemical species i , $\varepsilon_{i,j}$ is the standard emission factor for chemical species i in vegetation type j , and χ_j is the percentage of vegetation type j occupying a grid square.

Several vegetation environmental conditions are considered through the genetic factor expression reaction (2), when estimating the emission response, including light reaction by electron transfer, temperature response by in vivo enzyme activity, in vivo metabolite change, enzyme activity, and CO₂ levels. The main consideration is response to light, $\gamma_{P,i}$, which indicates the change of emission activity of chemical species i with light intensity, and is represented by the light-dependent fraction (LDF) and photosynthetic photon flux density (PPFD). Variable $\gamma_{T,i}$ indicates the change in the activity of chemical species i depending on temperature, expressed as its light-independent fraction (LIF); $\gamma_{A,i}$ is the discharge activity according to the age of the leaf—which is classified by MEGAN v2.1 into either New, Grow, Mature, or Old. The variable $\gamma_{SM,i}$ is the emission activity value according to the soil moisture content of the vegetation area, while $\gamma_{C,i}$ is the vegetation emission activity value according to atmospheric CO₂ concentration; $\gamma_{SM,i}$ and $\gamma_{C,i}$ are 1 for all chemical species apart from isoprene. The canopy environment coefficient (C_{CE}) and LAI are also used for calculating γ values:

$$\gamma_i = C_{CE} LAI \gamma_{P,i} \gamma_{T,i} \gamma_{A,i} \gamma_{SM,i} \gamma_{C,i}. \quad (2)$$

In addition, the PFT fraction and EF are used to calculate standard compound emission factors, expressed as grid emission factors, under standard conditions (temperature: 303 K; photosynthetic

photon density: 1000 $\mu\text{mol/s}$) [8]. Emission factors provided by MEGAN v2.1 [8] using various observations and experiments have been reported previously.

2.2. Vegetation Input Parameters

2.2.1. Plant Functional Type

PFT is a scheme used to classify vegetation and enables emissions estimation from vegetation species on a global basis. It is used in research land use and vegetation responses to climate change, and to classify vegetation according to climatological, phylogenetic, and biological characteristics. In general, PFT can be obtained from satellite data, vegetation lists, land cover maps, and ecosystem maps, but is mainly composed of satellite data [13]. In MEGAN v2.1, the PFT scheme involves 16 vegetation types, with each type designated using information on vegetation type and climate [8].

2.2.2. Leaf Area Index

Remote sensing, which has been widely used in recent vegetation and forest observational studies, provides information on a periodic basis, and is suitable for studying large areas at low cost [14]. Here, satellite-based remote sensing data are useful as the scope includes the entire Korean Peninsula—including North Korea, which cannot be easily accessed on the ground. Vegetation Index is a radiant value that represents the relative distribution and activity of green plants on the surface. LAI is a parameter related to plant physiology activity, and can be calculated using the normal distribution vegetation index (NDVI)—which is itself calculated using reflectance values from the red visible (Red) and near infrared (NIR) regions, for green plants [15,16]:

$$\text{NDVI} = \frac{\text{NIR} - \text{Red}}{\text{NIR} + \text{Red}} \quad (3)$$

NDVI is the most commonly used vegetation index; values range from -1 to 1 , with those between 0.1 and 0.6 being most common. The equation for calculating LAI using NDVI is shown as Equation (4) [17]:

$$\text{LAI} = 6.7537 \times \text{NDVI} + 0.8384 \quad (4)$$

2.3. BVOC Emissions Modeling Framework and Meteorological Input

The MEGAN modeling domain for BVOC emission estimation covered the Korean Peninsula (Figure 1). The modeling year was 2015, and meteorological data were produced by the Weather Research and Forecasting (WRF) model [18]. MEGAN v2.1 Emission Factor (EF), provided by the MEGAN development group, was used as the emission factor dataset, and detailed modeling framework information is listed in Tables 1 and 2.

In this study, four emission estimation cases were used to examine the effects of PFT and LAI on BVOCs estimation (Table 2). For Case 1, Moderate Resolution Imaging Spectroradiometer (MODIS) products were used for both PFT and LAI; for Case 2, PFT in South Korea was switched to merged local vegetation information (Local). Landcover information developed by the Ministry of Environment of Korea (KMOE, 2007) and the local forest type information from the Forest Research Institute of Korea (KFRI, 2016) were merged to develop the Local PFT. For Case 3, the Spatial and Temporal Adaptive Reflectance Fusion Model (STARFM) LAI and MODIS PFTs were used for both South and North Korea. For Case 4, Local PFT in South Korea and STARFM LAI in the domain were applied. The STARFM, a satellite data fusion method to develop high spatial and temporal resolution, was used to develop higher resolution (i.e., 30 m grid) LAI data [19].

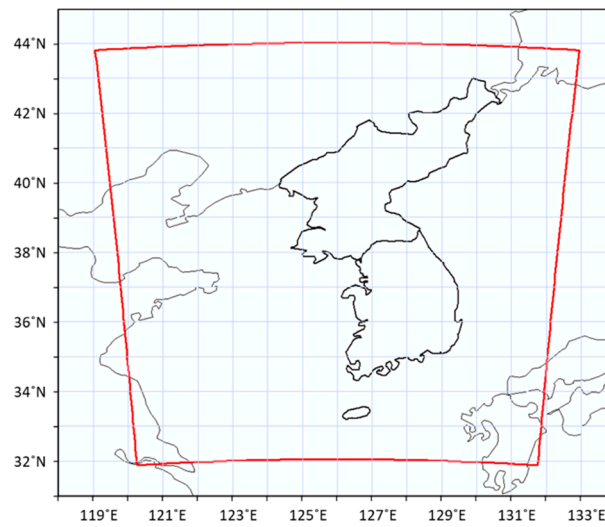


Figure 1. Definition of emissions modeling domain.

Table 1. Modeling parameter information.

Modeling Parameter	Content
Base year	2015
Grid (km)	18 × 18
MEGAN model version	MEGAN v2.1
Meteorological data	WRF v3.7.1 output
Emission factor data source	MEGAN EF v2.1

Table 2. Experiment cases.

Data	Domain	Case 1	Case 2	Case 3	Case 4
PFT	N.Korea	MODIS * (500 m grid)	MODIS *	MODIS *	MODIS *
	S.Korea		Local ** (50 m grid)		Local **
LAI	N.Korea	MODIS +	STARFM ++ (30 m grid)		
	S.Korea				

* MODIS land cover 2013 (MCD12Q1) [20]; ** Land Cover (KMOE, 2007) and Forest type map (KFRI, 2016) merged;
 + MODIS LAI 2015 (MCD15A2H) [21]; ++ STARFM LAI, 2018 [19].

3. Input Parameter Estimation over the Korean Peninsula

3.1. Composition of Modeling Input Parameters

3.1.1. Plant Functional Type

PFT data used in this study were MODIS MCD12Q1 products [8]. MCD12Q1 has a resolution of 500 m and provides 5 types of land cover, with Type 5, which provides 14 PFT types, being used in this study. Mapping of data with different classification schemes is required to apply the type to MEGAN v2.1, and so applying the MODIS Land Cover information into the MEGAN PFT format enabled mapping of 7 of the 16 vegetation categories in MEGAN [8]. Thus, MODIS PFT types 1–8 were mapped to MEGAN v2.1, being: Evergreen Needleleaf Trees, Evergreen Broadleaf Trees, Deciduous Needleleaf Trees, Deciduous Broadleaf Trees, Shrub, Grass, Cereal crops, and Broadleaf crops.

For South Korea, a local PFT was created using information from the Korea Ministry of Environment (MOE) Land cover map (KMOE, 2007) and Forest map (KFRI, 2016). The MOE land cover classification

divides land cover into seven categories: Developed area, Agricultural land, Forest area, Grassland, Wetland, Barren, and Watershed. The Forest map in this study had 51 landcover subcategories for 2016. Tables 3 and 4 list the MEGAN v2.1 PFT mapping format; their distributions are shown in Figure 2.

Table 3. Mapping Korea Landcover Level 2 into MEGAN v2.1 PFT (Vegetation only) [8].

Code	Land Cover Level 2	MEGAN v2.1 PFT	MEGAN Reclassification
210	Rice paddy		
220	Croplands		
230	Cultivation under structure	Crop	15
240	Orchards		
250	Other agricultural area		
310	Broadleaf forest	BT_DC_TEMP	7
320	Coniferous forest	NT_EG_TEMP	1
330	Mixed forest	NT_EG_TEMP and BT_DC_TEMP	77
410	Natural grasslands		
420	Artificial grasslands	GS_C3_WARM	14

Table 4. Mapping vegetation classes of the Korea Forest map into MEGAN v2.1 PFT [8].

Forest	Code	Classification	MEGAN v2.1 PFT	MEGAN Reclassification
Coniferous Forest	11	<i>Pinus densiflora</i>	NT_EG_TEMP	1
	12	<i>Pinus koraiensis</i>		
	13	<i>Larix kaempferi</i>	NT_DC_BORL	2
	14	<i>Pinus rigida</i>		
	15	<i>Pinus thunbergii</i>		
	16	<i>Abies holophylla</i>	NT_EG_TEMP	1
	17	<i>Chamaecyparis obtusa</i>		
	18	<i>Cryptomeria japonica</i>	NT_DC_BORL	2
	19	<i>Picea jezoensis</i>		
	20	<i>Torreya nucifera</i>	NT_EG_TEMP	1
Broadleaf Forest	21	<i>Ginkgo biloba</i>	NT_DC_BORL	2
	10	Needleleaf Trees	NT_EG_TEMP	1
	31	<i>Quercus acutissima</i>		
	32	<i>Quercus mongolica</i>		
	33	<i>Quercus variabilis</i>		
	34	Oak trees		
	35	<i>Alnus japonica</i>		
	36	<i>Acer pictum</i> subsp. <i>mono</i>		
	37	<i>Betula platyphylla</i> var. <i>japonica</i>		
	38	<i>Betula schmidtii</i>		
Evergreen Broadleaf Forest	39	<i>Castanea crenata</i>		
	40	<i>Fraxinus rhynchophylla</i>	BT_DC_TEMP	7
	41	<i>Carpinus laxiflora</i>		
	42	<i>Styrax japonicus</i>		
	43	<i>Juglans regia</i>		
	44	<i>Liriodendron tulipifera</i>		
	45	<i>Populus deltoides</i>		
	46	<i>Prunus serrulata</i> var. <i>spontanea</i>		
	47	<i>Zelkova serrata</i>		
	48	<i>Cornus controversa</i>		
Mixed Forest	49	<i>Robinia pseudoacacia</i>		
	30	Broadleaf Trees		
	61	<i>Quercus myrsinifolia</i>		
	62	<i>Castanopsis sieboldii</i>		
	63	<i>Cinnamomum camphora</i>	BT_EG_TEMP	5
	64	<i>Daphniphyllum macropodum</i>		
	65	<i>Dendropanax morbiferus</i>		
	66	<i>Eurya japonica</i>	SB_EG_TEMP	9
	67	<i>Machilus thunbergii</i>		
	68	<i>Neolitsea aciculata</i>	BT_EG_TEMP	5
Non-Forest	60	Evergreen broadleaf trees		
	77	Mixed forest	NT_EG_TEMP and BT_DC_TEMP	77
	92	Grasslands	GS_C3_WARM	14
	93	Croplands	CROP	15
	95	Orchards	CROP	15

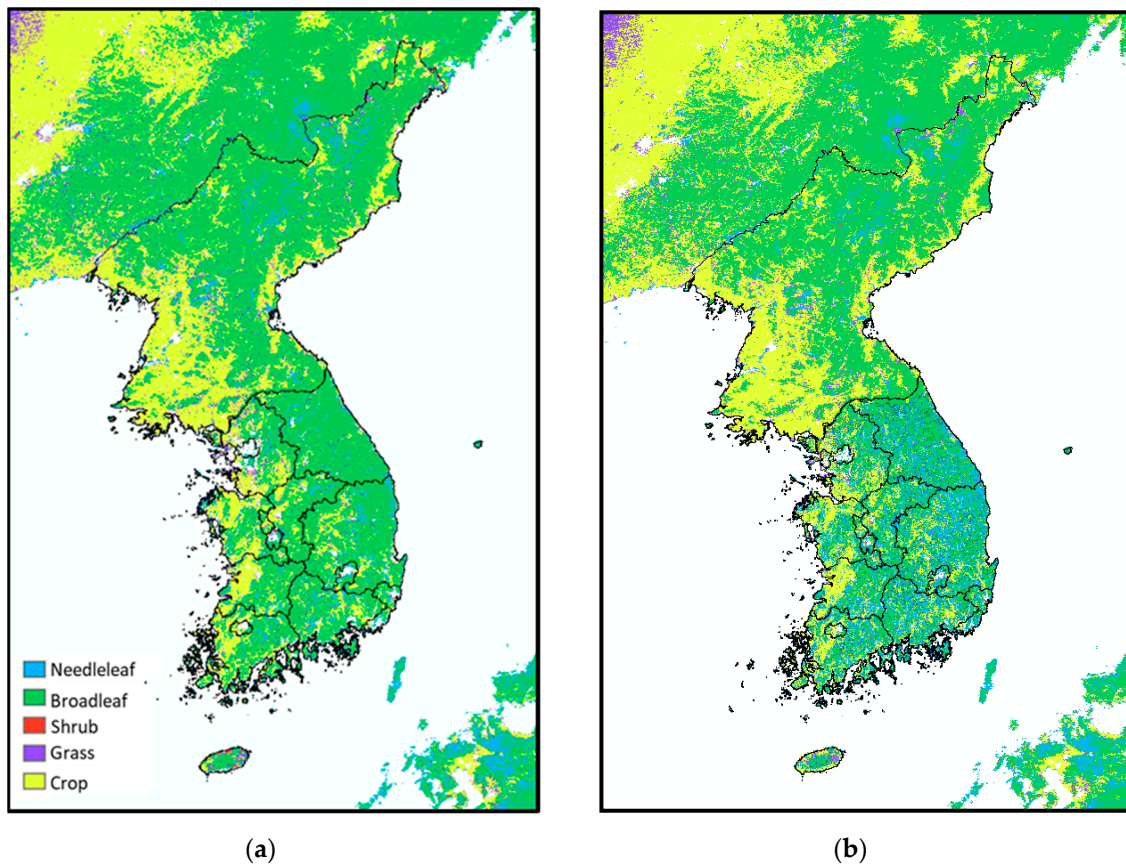


Figure 2. Land cover types for the Korean Peninsula: (a) Moderate Resolution Imaging Spectroradiometer (MODIS) Plant Functional Types (PFT); (b) local PFT.

The most abundant vegetation type in South Korea was identified as Broadleaf forests using both MODIS PFT and local PFT data, accounting for 53%, and 41%, respectively. In MODIS PFT, other major categories include Farmland (25%) and Needleleaf forest (6%); with local PFT, other major categories were Needleleaf forest (35%) and Farmland (20%). Compared with MODIS PFT, the largest change in local PFT data was an increase of 30% in Needleleaf forest, followed by a 13% difference for Broadleaf forest, 9% for non-vegetation, and there 6% less was categorized as Farmland (Figure 3).

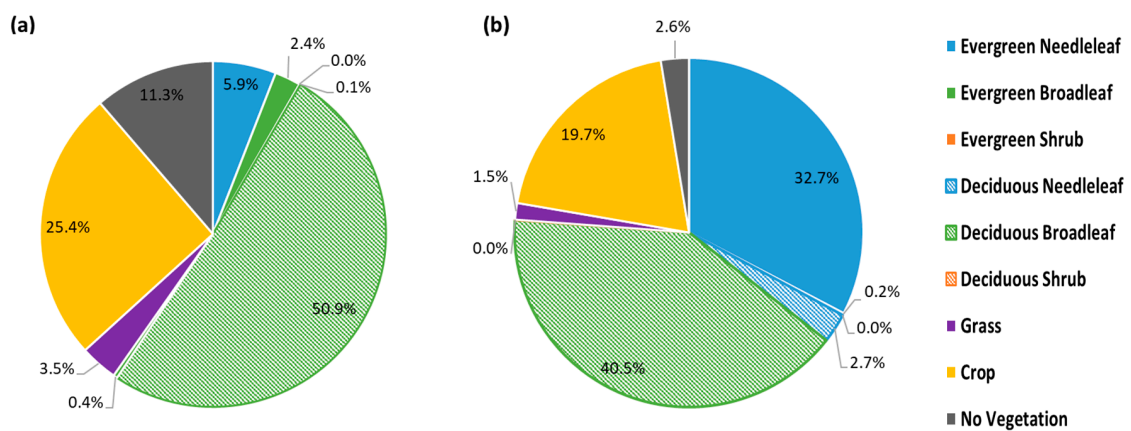


Figure 3. Plant Functional Type (PFT) distribution for South Korea: (a) Moderate Resolution Imaging Spectroradiometer (MODIS) PFT; (b) Local PFT.

In this study, we did not produce a local PFT for North Korea, as closed access makes it very difficult to collect ground-survey data for land cover, terrain, weather, etc. However, the MODIS PFT data itself is supportive in understanding North Korean biogenic emissions.

3.1.2. Leaf Area Index

Most BVOC studies use LAI created using the MODIS MCD15A2H product [15]. The MODIS LAI is composed of 46 data sets, created at 8-day intervals, each with a spatial resolution of 500 m. However, in order to produce LAI with higher spatial resolution than MODIS LAI, Landsat satellite data, with a spatial resolution of 30 m, were used. A total of 23 images were needed to cover the entire Korean Peninsula area, meaning that 276 Landsat satellite images were needed annually, to achieve monthly peninsula coverage. Weather interference meant that not all 276 images were usable, and so a simulated satellite data reconstruction method, known as STARFM (Spatial and Temporal Adaptive Reflectance Fusion Model), was used.

The STARFM method is a satellite data fusion technique, developed by Gao [22] to predict Landsat satellite data for a desired day, by fusing high spatial resolution Landsat satellite data with high temporal resolution MODIS sensor data. From the Landsat satellite, we used 11 band images with a resolution of 30 m for the whole Earth, while the MODIS product used in STARFM was MCD43A4, which provides 7 band images with 50 m resolution. Among these, NDVI was created using the relationship between the Red and NIR bands, and LAI was obtained through the relationship between NDVI and LAI [17].

MEGAN v2.1 LAI_v was calculated by dividing LAI (the leaf area index by grid using satellite data) by the vegetation share, F_v (5). LAI_v should have a value between 0 and 6 [6]:

$$LAI_v = LAI/F_v. \quad (5)$$

Our MODIS LAI used the MODIS MCD15A2H product [15], and our STARFM LAI used the LAI created using the STARFM method. As discussed, LAI is based on the reflectance of vegetation observed from the satellite, and LAIs for August and December in 2015 are shown in Figure 4. It can be seen that, overall, STARFM LAIs were higher than those from MODIS, which show fewer dark shaded areas (i.e., areas near zero).

For STARFM LAI, distinct edge effects were detected after creating a peninsular-wide mosaic. To produce the STARFM LAI for the Korean Peninsula, 23 pieces of LANDSAT data were required—although simultaneous imagery could not always be used owing to weather conditions (e.g., cloud interference). There were differences between some LANDSAT images owing to image timings, and these showed as a distinct edge. However, these differences should disadvantage emissions estimation much less than the benefit gained by using this more refined, higher resolution data.

Total LAIs, divided into South Korea and North Korea, are summarized in Table 5. Since LAI represents leaf activity, it shows seasonal change, with lower values in winter.

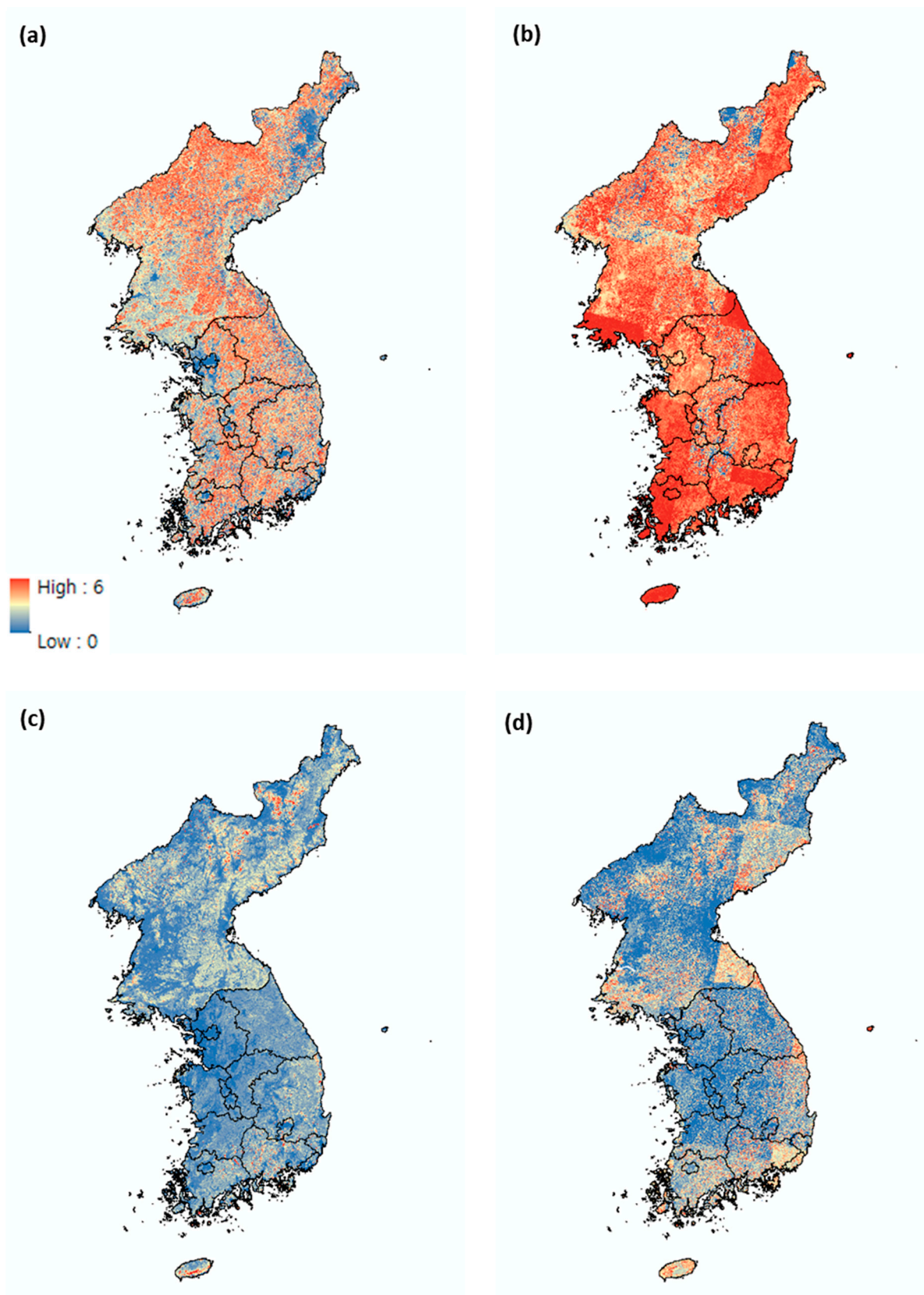


Figure 4. Summer to winter leaf area index (LAI) distributions for the Korean Peninsula, created using: (a) Moderate Resolution Imaging Spectroradiometer (MODIS) LAI (August); (b) Spatial and Temporal Adaptive Reflectance Fusion Model (STARFM) LAI (August); (c) MODIS LAI (December); (d) STARFM LAI (December).

Table 5. Regional Leaf Area Index (LAI) monthly totals [dimensionless].

	South Korea		North Korea	
	MODIS LAI (M)	STARFM LAI (S)	MODIS LAI (M)	STARFM LAI (S)
January	145	472	124	441
February	160	399	123	401
March	194	635	164	602
April	319	870	249	802
May	940	1174	915	1016
June	962	1403	1193	1319
July	971	1735	1255	1700
August	1053	1972	1386	1987
September	1001	1265	1072	1220
October	565	1090	307	1050
November	179	655	123	641
December	158	639	119	638
Total	6649	12,309	7030	11,816

3.2. Meteorological Input Data

Meteorological data were prepared by matching spatial ranges with the biogenic emissions model. The meteorological data used in this study were written every hour in 2015, the target period, using the WRF v3.7.1 model. The Meteorology-Chemistry Interface Processor (MCIP) was then used to convert this meteorological model output into a MEGAN-ready format. (Meteorology model configuration: Table 6).

Table 6. Meteorology model configuration [18].

Item	Description
WRF version	WRFv3.7.1
Resolution	18 × 18 km
Horizontal Grid	67 × 79
Vertical Grid	32 layer
NCEP data	1 degree, 6 hourly
Topography Data	30s USGS
Microphysics	WSM6 (WRF Single-Moment 6-Class)
Radiation physics	Shortwave: Dudhia scheme
	Longwave: RRTM scheme (Rapid Radiative Transfer Model)
PBL physics	YSU scheme
Cumulus physics	Kain-Fritsch (new Eta) scheme
Surface physics	Unified Noah land-surface model

We conducted verification by estimating the correlation between WRF meteorological model data used in MEGAN modeling and daily measurements (averaged from hourly measurements) from ground meteorological sites. Since there are no ground measurements available for North Korea, the selection of meteorological measurement site was limited to South Korea. There are 590 ground measurement sites (45 of which are manned) in South Korea. Seoul is one of the largest megacities in the world and the capital city of South Korea; it represents developed land in Korea. Chuncheon and Wonju are located in the Gangwon province, the province closest to North Korea, and represent a forest rich area. Chupungnyeong is located in the central hill of South Korea, and represents a forest rich area of the southern peninsula.

Correlations for temperature and radiation between model and weather station measurements are shown in Figures 5 and 6. Data distributions were calculated from daily averages during 2015.

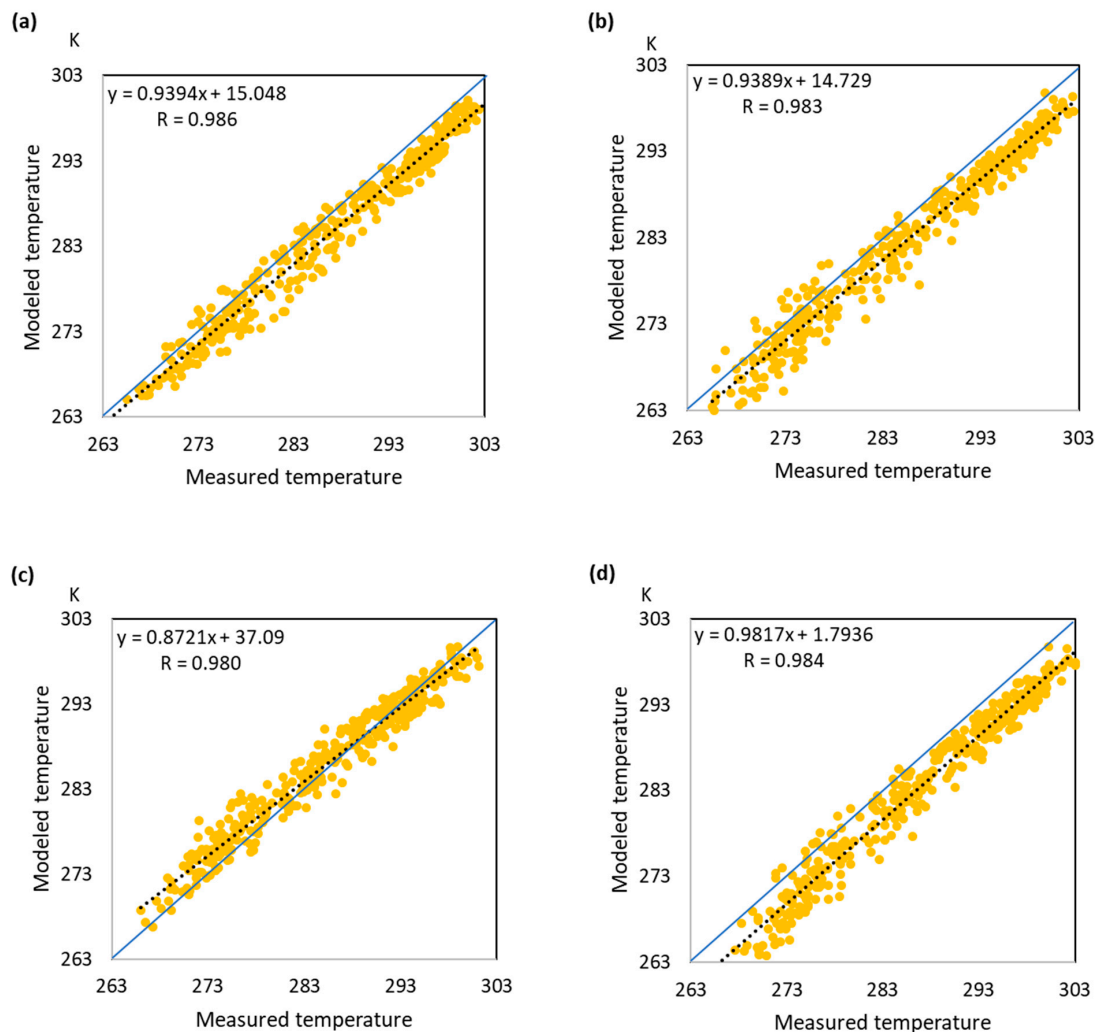


Figure 5. Correlation between Weather Research and Forecasting (WRF) model outputs and weather station measurements for temperature, at: (a) Seoul; (b) Chuncheon; (c) Chupungnyeong; and (d) Wonju.

For temperature (Figure 5), slopes were mostly >0.9 ; the WRF model results showed a tendency for slight underestimation, resulting in a negative bias. Correlation coefficient R showed high correlation (≥ 0.9). For solar radiation (Figure 6), slopes were $0.9\sim 1.1$; the WRF model had a tendency to overestimate, resulting in a positive bias. Correlation coefficient R showed high correlation (0.9). These results confirm that the WRF model produces reliable meteorological information for MEGAN modeling.

Tables 7 and 8 shows the results of WRF model verification for atmospheric temperature and solar radiation in each of the four regions, including Mean (M), Mean Bias (MB), Root Mean Square Error (RMSE), and Correlation Coefficient (R) values. From Table 7, the R of temperature data was very high ($0.98\sim 0.99$) but the model tended to underestimate temperature slightly (MBs of -3.47 K ~ -2.32 K, except for Chupungnyeong at 0.59 K). In contrast, Solar radiation (Table 8) showed relatively good R values ($0.86\sim 0.90$) but the model tended to overestimate solar radiation (MBs of $28.30\sim 45.51$ W/m 2 [$14.86\sim 23.76\%$]). One of the reason of this under/over estimation might be the grid (18 km) used for inter-comparison. While, this would have little impact on relative changes for our PFT and LAI cases, there remains a need to improve to absolute BVOC emission estimation performance.

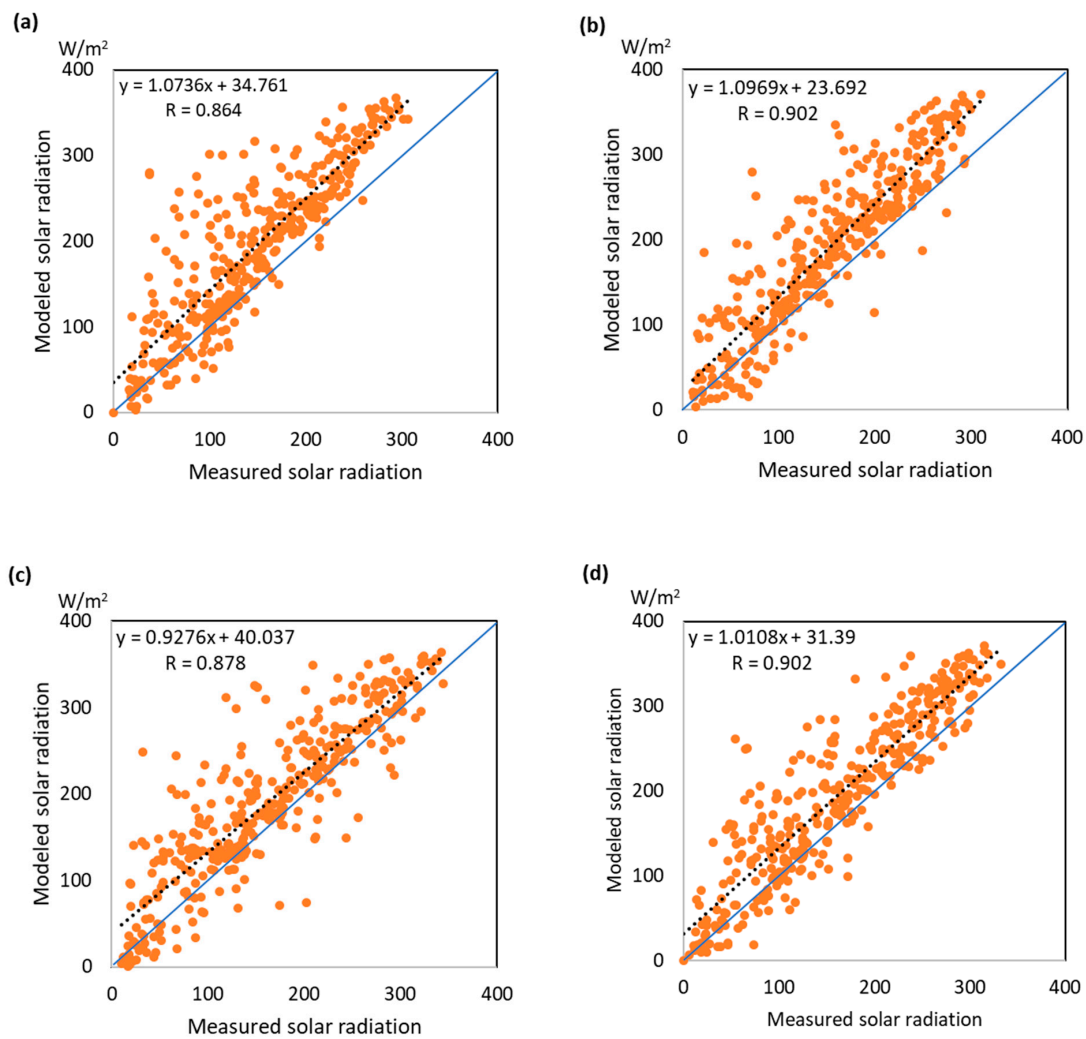


Figure 6. Correlation between Weather Research and Forecasting (WRF) model and weather station measurements of solar radiation, at: (a) Seoul; (b) Chuncheon; (c) Chupungnyeong; and (d) Wonju.

Table 7. Temperature mean (M), mean bias (MB), root-mean-square error (RMSE), and Correlation Coefficient (R) between the Weather Research and Forecasting (WRF) model and weather station measurements.

Temperature	M (K)	MB (K)	RMSE (K)	R
Seoul	284.44 (286.76)	−2.32	2.90	0.99
Chuncheon	283.00 (285.71)	−2.71	3.34	0.98
Chupungnyeong	285.94 (285.35)	0.59	2.07	0.98
Wonju	283.29 (286.76)	−3.47	3.91	0.98

(): Ground measurement data.

Table 8. Solar Radiation mean (M), mean bias (MB), root-mean-square error (RMSE) and Correlation Coefficient (R) between Weather Research and Forecasting (WRF) model and weather station measurements.

Solar Radiation	M (W/m ²)	MB (W/m ²)	RMSE (W/m ²)	R
Seoul	191.57 (146.06)	45.51	64.71	0.86
Chuncheon	189.47 (151.13)	38.33	56.02	0.90
Chupungnyeong	190.48 (162.18)	28.30	52.77	0.88
Wonju	194.54 (161.41)	33.13	52.40	0.90

(): Ground measurement data.

For BVOC emissions estimation, large seasonal variations would be expected in each scenario. To investigate the causes of seasonal differences, we analyzed LAI input data by comparing monthly average MODIS LAI and STARFM LAI data (Table 5) with 2-m-above-ground temperature (TEMP2) data (Figure 7). Both MODIS LAI and STARFM LAI showed low values in winter and high values in summer, with STARFM LAI values higher than those produced by MODIS LAI, particularly in winter, where values were 2~5 times higher (Table 5). For STARFM LAI, unlike MODIS LAI, LAI values were > 1 when TEMP2 was below freezing (273 K).

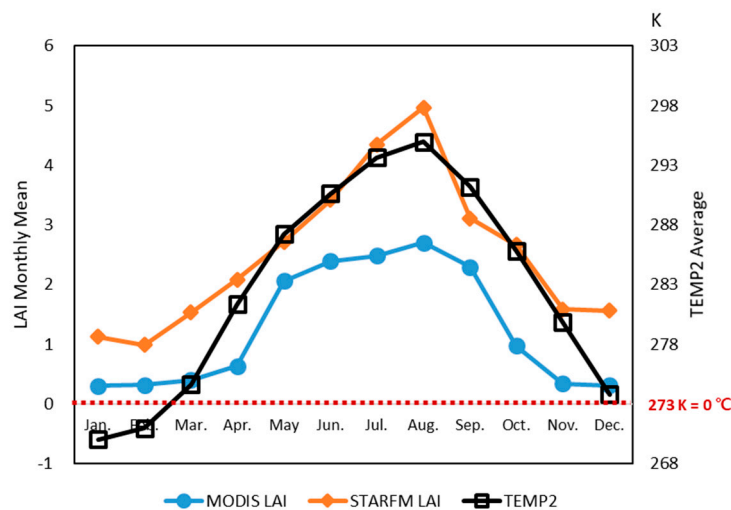


Figure 7. Comparison between Leaf Area Index (LAI) monthly mean estimates and 2-m-above-ground temperature (TEMP2) monthly Weather Research and Forecasting (WRF) model data averages for the Korean Peninsula.

According to [23], the NDVI can be positive, even below 273 K (0 °C). Furthermore, at 293 K (20 °C), the NDVI value can be as low as 0.4. Even at the same temperature, the NDVI value should be supported by precipitation data. The fact that NDVI is positive means that the LAI will also be positive, according to Equation (4). Since the average temperature in the Korean Peninsula is over 20 °C in summer, and rainfall is frequent (~83 days per year in 2015), the relationship between temperature, precipitation, and NDVI shows that STARFM LAI is a properly estimated input. In Siberia, vegetation is completely dominated by evergreen needleleaf spruce, fir, and pine; in below-freezing conditions, needleleaf forest that can tolerate cold, and evergreen forest that photosynthesizes regardless of season are required for NDVI and LAI to exhibit positive values [23].

From Figure 3, the composition of evergreen needleleaf forest increased from 5.9% in MODIS PFT to 32.7% in local PFT. With the local PFT, the ratio of evergreen forest to deciduous forest was three-fourth, which is more than four times that of MODIS PFT. From Figure 7, STARFM shows higher

LAI values than MODIS during winter months, which also supports the high composition of evergreen forest in South Korea

4. BVOC Emissions Estimation and Evaluation

4.1. BVOC Emissions Estimation

Using the four modelling approaches, monthly vegetation emission estimates were calculated for isoprene and monoterpenes emissions (Tables 9 and 10). Overall, monthly emissions were low in winter and high in summer, as expected, and there was also an overall difference in emission amounts. South Korea exhibited its highest emission levels in August, and North Korea showed its highest emissions in July; mean temperatures and the monsoon are potential causes of these differences.

Table 9. Monthly biogenic emissions in South Korea (Gg/period).

Month	Isoprene				Monoterpenes			
	Case 1	Case 2	Case 3	Case 4	Case 1	Case 2	Case 3	Case 4
January	0.36	0.30	0.56	0.62	0.42	0.66	0.87	1.78
February	0.68	0.55	1.00	0.98	0.52	0.78	0.85	1.64
March	3.50	2.72	5.12	4.55	1.20	1.78	2.20	3.98
April	10.00	2.72	14.50	12.36	3.34	1.78	4.38	7.57
May	49.77	38.98	50.23	41.95	10.05	14.83	9.84	16.49
June	73.63	57.76	72.35	60.97	11.80	17.50	13.05	21.89
July	88.42	70.12	94.54	80.71	15.81	23.77	17.08	29.05
August	118.83	95.98	123.13	109.56	18.64	28.62	20.08	35.91
September	50.21	42.01	50.88	48.85	10.50	16.46	11.19	21.26
October	18.27	15.32	19.28	19.07	5.30	8.33	6.31	12.35
November	1.88	1.57	2.92	2.99	1.43	2.22	2.75	5.41
December	0.55	0.45	0.97	1.04	0.70	1.07	1.46	2.98
Total	416.11	328.49	435.48	383.65	79.71	117.78	90.05	160.33

Table 10. Monthly biogenic emissions in North Korea (Gg/period).

Month	Isoprene		Monoterpenes	
	Case 1	Case 4	Case 1	Case 4
January	0.08	0.18	0.17	0.46
February	0.17	0.36	0.18	0.48
March	1.03	2.15	0.52	1.25
April	6.73	11.80	1.90	3.43
May	34.56	41.13	8.11	8.14
June	62.85	65.52	10.43	11.82
July	84.49	92.40	13.97	16.26
August	67.80	80.67	13.73	15.36
September	33.11	35.71	7.44	8.59
October	6.25	8.89	2.30	3.96
November	0.46	1.04	0.46	1.44
December	0.10	0.30	0.23	0.79
Total	297.63	340.16	59.43	71.98

In South Korea, four cases of model emissions (Case 1, Case 2, Case 3, and Case 4) were estimated, based on a combination of input data (Tables 1 and 2). Isoprene emissions were lowest in January (0.36, 0.30, 0.56, and 0.62 Gg/month for the respective cases). In August, the highest emission month, values were 118.83, 95.98, 123.13, and 109.56 Gg/month for the respective cases. For monoterpenes, the month with the lowest emissions was classified according to the type of LAI. When using MODIS LAI (Case 1, Case 2), January was the lowest month (0.42 and 0.66 Gg/month, respectively). When STARFM LAI (Case 3, Case 4) was used, emissions were 0.85, and 1.64 Gg/month, respectively, in February.

Monoterpene emissions from PFT showed the opposite trend to that of isoprene emissions. The lowest isoprene emission figure was 328.49 Gg/year (Case 2), and the highest was 435.48 Gg/year (Case 3). The lowest monoterpene emission reading was 79.71 Gg/year (Case 1) and the highest was 160.33 Gg/year (Case 4).

The emission estimate amounts differed between cases and species. When the LAI changed from MODIS LAI to STARFM LAI, emissions of both isoprene and monoterpenes increased (by 50% for isoprene and 70% for monoterpenes). When the PFT changed from MODIS PFT to Local PFT (South Korea), isoprene emissions decreased by 20%, while monoterpenes emissions increased by 60%.

When using the same LAI, the use of Local PFT in cases 2 and 4 reduced isoprene emissions and increased monoterpenes emissions because the composition of the PFT had changed (Figure 3). The portion of broadleaf trees decreased by 10% in the local PFT compared with the MODIS PFT, and the needleleaf trees increased by ~6 times. When we examined the Emission Factor (EF) for each PFT used in MEGANv2.1 [8], isoprene EF decreases by 95% when changing from broadleaf to needleleaf trees; in monoterpenes, it increases by 50% for the same change. For this reason, when the Local PFT was used, isoprene emissions were reduced, while monoterpene emissions increased.

North Korea produced two emission cases (Case 1, Case 4) to changes in LAI (Table 10). The lowest monthly isoprene emission estimates were for January (0.08 Gg/month in Case 1, and 0.18 Gg/month in Case 4), and the highest were in July (84.49 and 92.40 Gg/month, for cases 1 and 4, respectively). Total annual emission estimates for North Korea (Case 1 and Case 3) were 297.63 and 340.16 Gg/year, respectively, with Case 4 estimates 14% higher than those of Case 1 values.

For monoterpenes, January produced the smallest emission estimate in North Korea, with Case 1 yielding an estimate of 0.17 Gg/month, and Case 4 yielding 0.46 Gg/month. The largest monthly monoterpene emission estimates were in July, at 13.97 Gg/month and 16.26 Gg/month. Comparing Case 1 (59.43 Gg/year) to Case 4 (71.98 Gg/year). Case 4 values were 21% larger than Case 1 monoterpene emissions in North Korea. In most cases, North Korea showed the highest emissions in July (Table 10). Unlike the rest of the Korean Peninsula, temperatures in North Korea were higher in July than in August, causing North Korea's BVOC emissions to peak then, rather than in August.

Case 4 BVOC emission estimates were –8–101% higher than Case 1 estimates, depending on whether isoprene or monoterpene data were reviewed. However, when compared on a monthly basis, the differences were larger, with cold season estimates (January–March and November–December) more than twice as high; between May and August, differences were approximately 10%. In the cold season, local PFT and STARFM LAI estimates were relatively high compared with those of MODIS PFT and LAI, as described in Section 3.1, reflecting a relative increase in Evergreen needle leaf forests in the local PFT.

4.2. Comparison with Inverse Estimates of BVOC Emissions

We used inverse emissions estimates from GlobEmission [24] and observational data for 2015 to compare vegetation emissions from the Korean Peninsula. The isoprene emissions, provided by GlobEmission, were estimated using HCHO (formaldehyde) column concentrations, measured with an OMI (Ozone Monitoring Instrument) sensor. As of June 2020, GlobEmission provides monthly Global Biogenic Isoprene emissions for 2005–2014 (but not 2015). To compare isoprene emissions over the Korean Peninsula, the results of this study were compared with GlobEmission estimations for 2014. To make this comparison, we performed WRF modeling for 2014.

South Korea's monthly isoprene emissions in 2014 and 2015 were compared using Case 4 (Figure 8). Emissions in 2014 were 349.88 Gg/yr, 10% less than in 2015. Monthly variations showed greater variation than annual estimates. Usually, August has the highest temperature and humidity, which induces high vegetation emissions. In August 2014, isoprene emissions were 37% less than those of 2015 (Figure 8). In 2014, two large typhoons affected South Korea, causing heavy rain in most parts of the country. Therefore, the average temperature was lower and the average precipitation was higher than the 30-year average (year 1981–2010). Furthermore, more days of precipitation were recorded [25].

Low daylight hours (74% of a normal year), were reflected in the lower isoprene emissions in 2014. As such, emissions in August 2014 and 2015 showed a marked difference; however, Figure 9 shows that monthly emissions in 2014 were well estimated by the bottom-up modeling, since emissions showed a similar trend to GlobEmission.

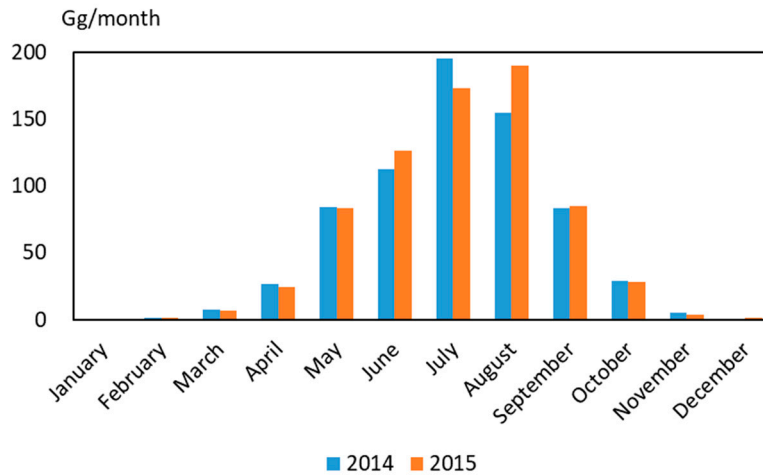


Figure 8. Modeling (bottom-up) isoprene emissions in South Korea (Case 4).

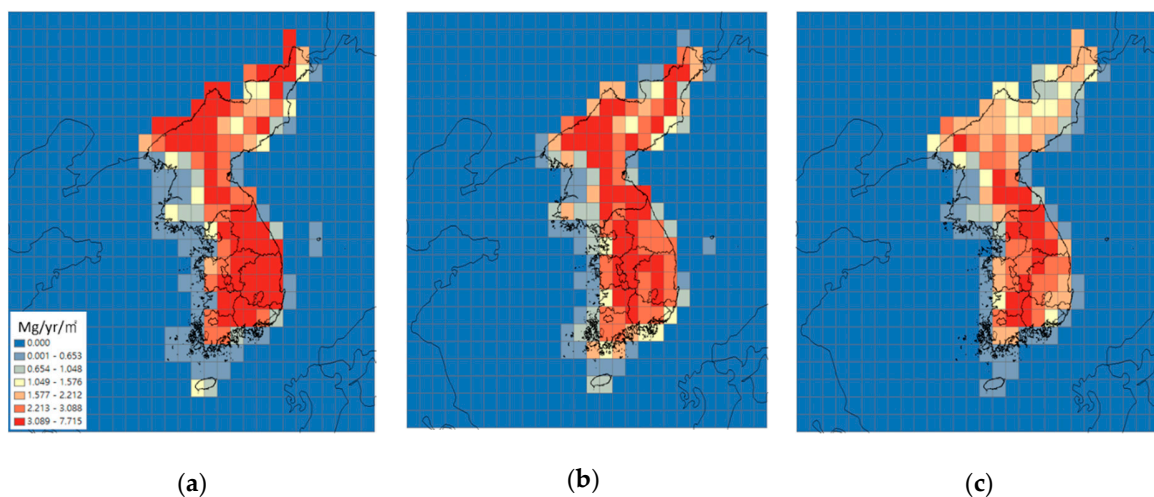


Figure 9. Distribution of isoprene emissions in 2014: (a) bottom-up emissions (Case 1); (b) bottom-up emissions (Case 4); (c) inverse emission estimates from GlobEmission [24].

Figure 9 shows 2014 bottom-up isoprene emissions estimated in this study and the inverse emission (GlobEmission) distributions. Using the bottom-up isoprene estimates for South Korea, Case 1 emission estimates for 2014 (373.85 Gg/year) were lower than those for 2015 (416.11 Gg/year); Case 4 emissions estimates showed the same trend (349.88 Gg/year for 2014 and 383.65 Gg/year for 2015). This reflects the two large typhoons in August 2014. The GlobEmission estimate for 2014 (260.71 Gg/year) was close to the Case 4 estimate (134%). For North Korea, the isoprene emission estimates for 2015 were lower than those of 2014. In the Case 1, annual emissions for 2015 were 297.63 Gg/year vs. 332.82 Gg/year for 2014. For Case 4, emissions were 340.16 Gg/ in 2015 and 351.83 Gg/year in 2014. For bottom-up to top-down inter-comparison, Case 1 values were closer (125%) than Case 4 values to the 2014 GlobEmission emission value (267.28 Gg/year).

Monthly isoprene emissions in South Korea (a) and North Korea (b) are inter-compared with GlobEmissions in Figure 10. In general, bottom-up emissions showed similar monthly variations to

GlobEmission emissions in 2014, with the highest emissions in July. In South Korea, the LAI and PFT for Case 1 and Case 4 were different, causing a difference in monthly emissions between these cases. Monthly emissions from May to July, when vegetation is active, showed a noticeable difference between cases, with estimations close to those of GlobEmissions in Case 4. Although emission amounts for Case 4 were larger than those of GlobEmission values (134%), the difference was smaller, considering that solar radiation shows a positive bias of ~15–20 (Table 8). However, for North Korea, the difference between Case 1 and Case 4 was only observed for LAI, with no significant difference in emissions (7%) or patterns.

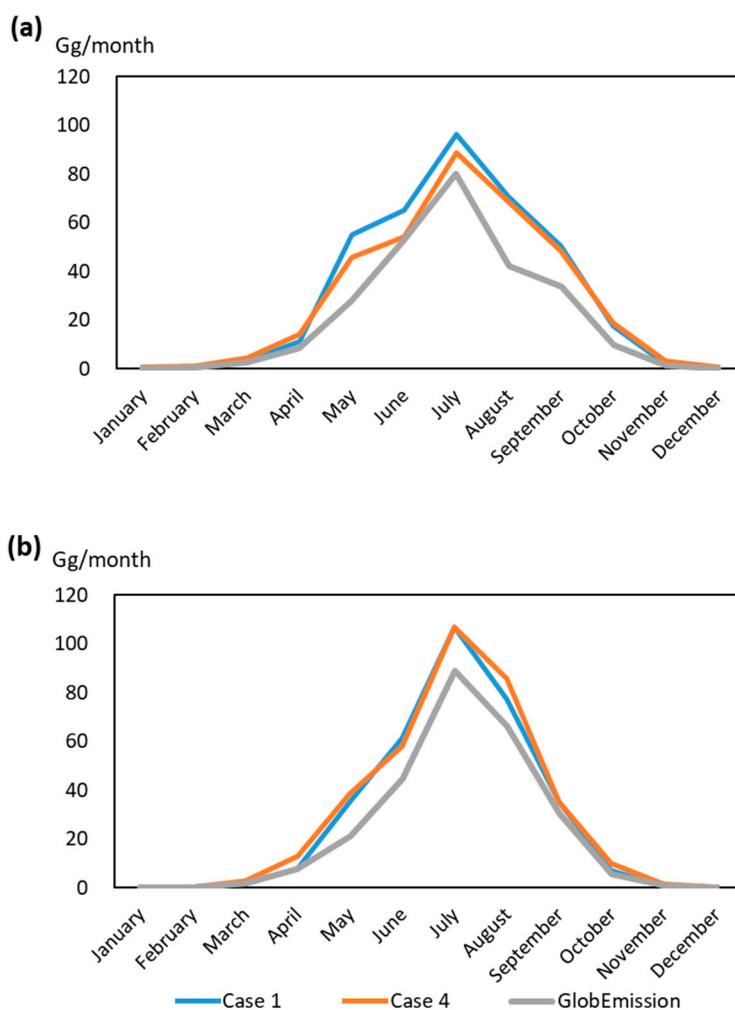


Figure 10. Monthly variations in modeling (bottom-up) isoprene emissions and GlobEmission (inverse) emissions in 2014: (a) South Korea; (b) North Korea.

To compare emission estimation performances, bottom-up emissions for Case 1 and Case 4 were plotted with those of GlobEmission (Figure 11). For Case 1, the slope was 1.59, and for Case 4, the slope was 1.09, with bottom-up emission results showing a tendency towards slight overestimation (i.e., positive bias). The correlation coefficient R showed high correlation (0.90). Even though both bottom-up emission cases overestimated isoprene emissions in June and July of 2014 for South Korea (Table 11), the degree of agreement was much better for Case 4, which is consistent with the previous analysis.

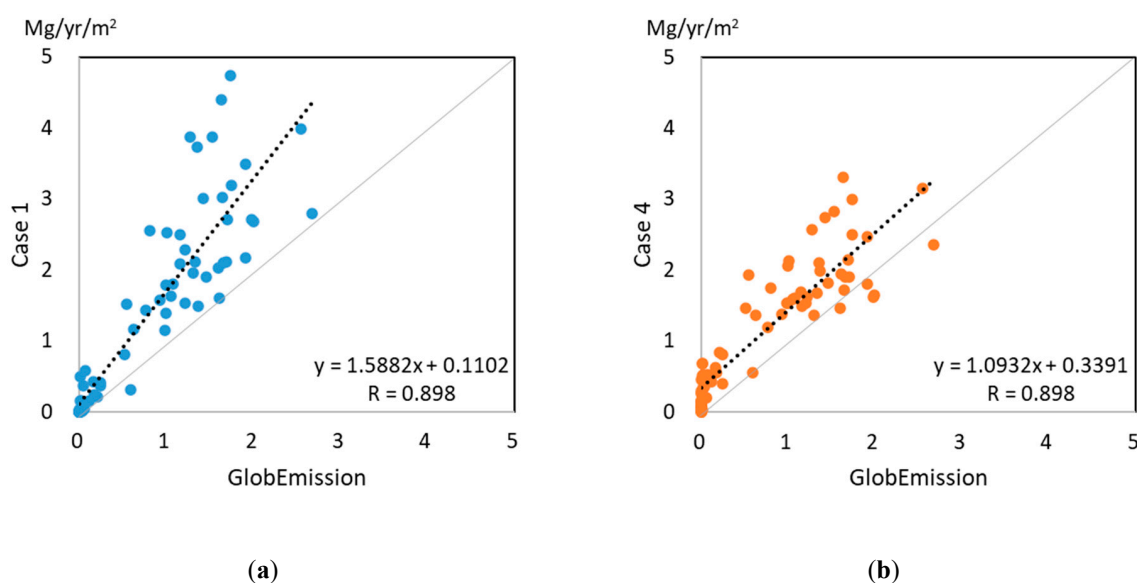


Figure 11. Correlation between modeling (bottom-up) and inverse (top-down) emissions in South Korea in June and July 2014: (a) Case 1; (b) Case 4.

Table 11. Statistical performance measures (Mean, MB, RMSE, and R) between bottom-up emissions and GlobEmission for South Korea in June and July 2014.

Emissions	M (Mg/yr/ m ²)	MB (Mg/yr/ m ²)	RMSE (Mg/yr/ m ²)	R
GlobEmission	0.76			
Case 1	1.30	0.55	0.92	0.90
Case 4	1.18	0.42	0.59	0.90

5. Conclusions

The purpose of this study was to understand changes in BVOC emissions estimates using different input data. The biogenic emissions model used was MEGAN v2.1, and the target VOC species were isoprene and monoterpenes. Data related to vegetation were: (1) MODIS PFT and LAI; (2) local PFT, which is a fusion of Korean land cover and forest mapping, and (3) LAI using STARFM, a satellite data convergence algorithm. An important input dataset, meteorology, was obtained by taking a full year of WRF modeling and converting it using the MCIP. BVOC emission input data series were prepared by converting each of the above datasets into a form suitable for MEGAN v2.1.

MEGAN modeling was conducted for 2015 for four different cases. For Case 1, estimates of 416.11 Gg/year isoprene and 79.71 Gg/year monoterpenes were derived for South Korea, and 297.63 Gg/year and 59.43 Gg/year, respectively, for North Korea. For Case 2, estimates of 328.49 Gg/year isoprene and 117.78 Gg/year monoterpenes were derived for South Korea only. For Case 3, 435.48 Gg/year isoprene and 90.05 Gg/year monoterpenes were estimated for South Korea only. Finally, for Case 4, 383.65 Gg/year isoprene and 160.33 Gg/year monoterpenes were estimated for South Korea, while 340.16 Gg/year and 71.98 Gg/year, respectively, were estimated for North Korea. Emissions estimates between Case 1 and the other cases varied by -21 – 101% for isoprene and monoterpenes. Changes in LAI increased emission estimates for both isoprene and monoterpenes, while changes in PFT led decreased isoprene emissions and increased monoterpenes emissions estimates.

We attempted a comparison with biogenic isoprene emission data provided by GlobEmission, but could not make a direct comparison, as GlobEmission only provides emissions information up to 2014. For direct inter-comparison, we ran the WRF model for 2014 and performed emissions evaluation using inverse emissions estimation from GlobEmissions. For Case 1, emission estimates for

2014 were 373.85 Gg/year for South Korea and 332.82 Gg/year for North Korea, which is 143% and 125% of the GlobEmission isoprene emissions, respectively. For Case 4, bottom-up emissions were 349.88 Gg/year for South Korea and 351.83 Gg/year for North Korea, which is 134% of GlobEmissions for South Korea and 132% for North Korea. Correlation analysis and monthly inter-comparison indicate that our bottom-up emissions represent reasonable spatial and temporal variations using Case 4, but generally overestimated the amount of BVOCs.

We have tested BVOCs emissions estimation over the Korean Peninsula using multiple PFTs and LAIs. The results indicate that the enhancement of BVOC model input data using local PFT and refined LAI can effectively improve BVOC emissions estimation accuracy. However, the accuracy of the meteorological model requires improvement; currently, it is a major reason for uncertainties owing to overestimation of solar radiation.

In future study, the following improvements will be made. First, BVOCs emission factors require improvement by using more locally developed ones. Second, LAI estimation formulae need to be improved to be more specific to each PFTs. Third, soil moisture needs to be improved, especially for monoterpenes, since our present estimation does not include the effect of drought on terpenoid emissions. Fourth, understanding the performance of monoterpenes emissions estimation by direct evaluation using measurement data.

Author Contributions: Conceptualization, J.-H.W. and Y.K.; methodology, Y.E. and M.J.; formal analysis, Y.J.; resources, Y.E. and M.J.; data curation, Y.J.; writing—original draft preparation, Y.J.; writing—review and editing, J.-H.W. and Y.K.; supervision, J.-H.W., J.-B.L. and J.-H.L.; funding acquisition, J.-B.L. and J.-H.L. All authors have read and agreed to the published version of the manuscript.

Funding: This research was supported by the National Strategic Project-Fine Particles of the National Research Foundation of Korea, funded by the Ministry of Science and ICT, the Ministry of Environment, and the Ministry of Health and Welfare (grant number: NRF-2017M3D8A1092022); by the Korea Environment Industry & Technology Institute (KEITI), through its Public Technology Program, based on Environmental Policy Program, funded by Korea Ministry of Environment (grant number: 2019000160007); and by a grant from the National Institute of Environment Research (NIER), funded by the Ministry of Environment (MOE) of the Republic of Korea (NIER-2012-00-02-136).

Acknowledgments: The authors acknowledge the use of BIRA-IASB satellite derived isoprene emission data from www.globemission.eu.

Conflicts of Interest: The authors declare no conflict of interest.

References

1. Karl, T.; Guenther, A.; Sprig, C.; Hansel, A.; Fall, R. Seasonal variation of biogenic VOC emissions above a mixed hardwood forest in northern Michigan. *Geophys. Res. Lett.* **2003**, *30*, 2186. [[CrossRef](#)]
2. Pierce, T.E.; Geron, C.; Bender, L.; Dennis, R.; Tonnesen, G.; Guenther, A. Influence of increased isoprene emissions on regional ozone modeling. *J. Geophys. Res.* **1998**, *103*, 25622–25629. [[CrossRef](#)]
3. Morris, R.E.; Koo, B.; Guenther, A.; Yarwood, G.; McNally, D.; Tesche, T.W.; Tonnesen, G.; Boylan, J.; Brewer, P. Model sensitivity evaluation for organic carbon using two multi-pollutant air quality models that simulate regional haze in the southeastern United States. *Atmosp. Environ.* **2006**, *40*, 4960–4972. [[CrossRef](#)]
4. Tsigaridis, K.; Kanakidou, M. Secondary organic aerosol importance in the future atmosphere. *Atmosp. Environ.* **2007**, *41*, 4682–4692. [[CrossRef](#)]
5. Cho, K.-T.; Kim, J.-C.; Hong, J.-H. A Study on the Comparison of Biogenic VOC (BVOC) Emissions Estimates by BEIS and CORINAIR Methodologies. *J. Korean Soc. Atmosp. Environ.* **2006**, *22*, 167–177.
6. NIER (National Institute of Environmental Research). *KORUS-AQ Rapid Science Synthesis Report*; NIER: Incheon, Korea, 2017.
7. Guenther, A.; Karl, T.; Harley, P.; Wiedinmyer, C.; Palmer, P.I.; Geron, C. Estimates of global terrestrial isoprene emissions using MEGAN (Model of Emissions of Gases and Aerosols from Nature). *Atmosp. Chem. Phys.* **2006**, *6*, 3181–3210. [[CrossRef](#)]
8. Guenther, A.B.; Jiang, X.; Heald, C.L.; Sakulyanontvittaya, T.; Duhl, T.; Emmons, L.K.; Wang, X. The Model of Emissions of Gases and Aerosols from Nature version 2.1 (MEGAN v2.1): An extended and updated framework for modeling biogenic emissions. *Geosci. Model Dev.* **2012**, *5*, 1471–1492. [[CrossRef](#)]

9. Messina, P.; Lathière, J.; Sindelarova, K.; Vuichard, N.; Granier, C.; Ghattas, J.; Cozic, A.; Hauglustaine, D.A. Global biogenic volatile organic compound emissions in the ORCHIDEE and MEGAN models and sensitivity to key parameters. *Atmosp. Chem. Phys.* **2016**, *16*, 14169–14202. [[CrossRef](#)]
10. Henrot, A.-J.; Stanelle, T.; Schröder, S.; Siegenthaler, C.; Taraborrelli, D.; Schultz, M.G. Implementation of the MEGAN (v2.1) biogenic emission model in the ECHAM6-HAMMOZ chemistry climate model. *Geosci. Model Dev.* **2017**, *10*, 903–926. [[CrossRef](#)]
11. Sindelarova, K.; Granier, C.; Bouarar, I.; Guenther, A.; Tilmes, S.; Stavrakou, T.; Müller, J.-F.; Kuhn, U.; Stefani, P.; Knorr, W. Global data set of biogenic VOC emissions calculated by the MEGAN model over the last 30 years. *Atmosp. Chem. Phys.* **2014**, *14*, 9317–9341. [[CrossRef](#)]
12. Han, K.M.; Park, R.S.; Kim, H.K.; Woo, J.H.; Kim, J.; Song, C.H. Uncertainty in biogenic isoprene emissions and its impacts on tropospheric chemistry in East Asia. *Sci. Total Environ.* **2013**, *463*, 754–771. [[CrossRef](#)] [[PubMed](#)]
13. Oleson, K.W.; Bonan, G.B. The effects of remotely-sensed plant functional type and leaf area index on simulations of boreal forest surface fluxes by the NCAR land surface model. *J. Hydrometeorol.* **2000**, *1*, 431–446. [[CrossRef](#)]
14. Jensen, J.R. *Remote Sensing of the Environment: An Earth Resource Perspective*; Pearson: Upper Saddle River, NJ, USA, 2007.
15. Huete, A.; Justice, C.; Leeuwen, W. *Modis Vegetation Index Algorithm Theoretical Basis Document*; Department of Environmental Sciences; University of Virginia: Charlottesville, VA, USA, 1999.
16. Rouse, J., Jr.; Haas, R.H.; Schell, J.A. In *Third Earth Resources Technology Satellite-1 Symposium- Volume I: Technical Presentations*; NASA SP-351; Freden, S.C., Mercanti, E.P., Becker, M.A., Eds.; NASA: Washington, DC, USA, 1974; p. 309. 1994p.
17. Schiffman, B.; Basson, G.; Lue, E.; Ottman, D.; Hawk, A.; Ghosh, M.; Melton, F.; Schmidt, C.; Skiles, J.W. Estimation of leaf area index (LAI) through the acquisition of ground truth data in Yosemite national park. In Proceedings of the ASRPS 2008 Annual Conference, Portland, OR, USA, 28 April–2 May 2008.
18. WRF Model Users' Page. Available online: <http://www2.mmm.ucar.edu/wrf/users/> (accessed on 20 March 2018).
19. Lee, J.M. Monthly LANDSAT LAI Generation in Korean Peninsula. Master's Thesis, Konkuk University, Seoul, Korea, 2018.
20. LPDAAC (Land Processes Distributed Active Archive Center). Available online: https://lpdaac.usgs.gov/dataset_discovery/modis/modis_products_table/mcd12q1 (accessed on 25 July 2018).
21. LAADS (Level-1 and Atmosphere Archive & Distribution System). Available online: <https://ladsweb.modaps.eosdis.nasa.gov/missions-and-measurements/products/lai-and-fpar/MCD15A2H> (accessed on 25 July 2018).
22. Gao, F.; Masek, J.; Hall, F. On the Blending of the Landsat and MODIS Surface Reflectance: Predicting Daily Landsat Surface Reflectance. *IEEE Trans. Geosci. Remote Sens.* **2006**. [[CrossRef](#)]
23. Suzuki, R.; Nomaki, T.; Yasunari, T. Spatial Distribution and its Seasonality of Satellite-derived Vegetation Index (NDVI) and Climate in Siberia. *Int. J. Climatol.* **2001**, *21*, 1321–1335. [[CrossRef](#)]
24. Bauwens, M.; Stavrakou, T.; Müller, J.-F.; De Smedt, I.; Van Roozendaal, M.; van der Werf, G.R.; Wiedinmyer, C.; Kaiser, J.; Sindelarova, K.; Guenther, A. Nine years of global hydrocarbon emissions based on source inversion of OMI formaldehyde observations accepted in *Atmos. Chem. Phys.* **2016**. [[CrossRef](#)]
25. KMA (Korea Meteorological Administration). *Monthly Weather Report 2014*; KMA: Seoul, Korea, 2014.

